Liquid-solid transitions in the three-body hard-core model

Tommaso Comparin[(a)], Sebastian C. Kapfer[(b)] and Werner Krauth[(c)]

Laboratoire de Physique Statistique, École Normale Supérieure/PSL Research University, UPMC, Université Paris Diderot, CNRS, 24 rue Lhomond, 75005 Paris, France

arXiv:1410.1454v2 [cond-mat.stat-mech] 5 Feb 2015

PACS 05.20.Jj – Statistical mechanics of classical fluids
PACS 64.70.dj – Melting of specific substances

Abstract – We determine the phase diagram for a generalisation of two-and three-dimensional hard spheres: a classical system with three-body interactions realised as a hard cut-off on the mean-square distance for each triplet of particles. Quantum versions of this model are important in the context of the unitary Bose gas, which is currently under close theoretical and experimental scrutiny. In two dimensions, the three-body hard-core model possesses a conventional atomic liquid phase and a peculiar solid phase formed by dimers. These dimers interact effectively as hard disks. In three dimensions, the solid phase consists of isolated atoms that arrange in a simple-hexagonal lattice.

Introduction. – In many fields of physics, interactions between particles are accurately described through pair potentials. These potentials can be long-range or short-range, and may combine attractive and repulsive components, as in the Lennard-Jones interaction. The minimal model for pairwise-interacting systems is the hard-sphere potential, which has played a central role in statistical mechanics and computational physics, and is also a prominent topic in mathematical research [1–3].

In a number of cases, two-body potentials are insufficient to describe complex physical behaviour. A notorious example are nuclear forces, where three-body interactions have long been discussed [4,5]. Explicit three-body terms appear also in spin glasses, as in the well-known p-spin model [6].

Recently, three-body potentials were studied in cold atomic quantum gases. One proposed route to enhance their effects consists in suppressing the pair interactions [7]. The unitary Bose gas at low temperature represents another situation where three-body physics is relevant. For some bosonic atoms, the Feshbach-resonance technique allows to reach the *unitary* regime, where the two-particle scattering length diverges, and an additional length scale is provided by a three-body parameter. Experiments in this regime have lead to direct evidence of the Efimov effect [8–11], a spectacular manifestation of three-body physics in the quantum realm. This has triggered a massive experimental and theoretical effort on the study of this strongly-interacting system [12–18].

The above considerations motivate the study of a minimal model of three-body interactions. In the current work, we consider a classical system in which each triplet (i, j, k) of particles interacts through the potential

$$V_3(R_{ijk}) = \begin{cases} \infty & \text{if } R_{ijk} < R_0 \\ 0 & \text{if } R_{ijk} > R_0 \end{cases} , \qquad (1)$$

where $R_{ijk}^2 = (r_{ij}^2 + r_{jk}^2 + r_{ki}^2)/3$. The interaction term of eq. (1) explicitly appears in recent theoretical models of the unitary Bose gas [15,17], where it prevents the collapse [19] of the quantum-mechanical wave function. In the corresponding experimental system, the three-body parameter R_0 is related to the length scale of the van der Waals interactions [20–22].

Among the many generalisations of the hard-sphere model (*e. g.* to aspherical and polydisperse objects, or to dimensions different from three), the three-body hard-core model has not – to our knowledge – been studied before.

As for the hard-sphere model, the phase diagram of the three-body hard-core model is independent of temperature, and transitions are driven purely by entropy. The crucial distinction of the three-body hard-core model is that two particles can exist at zero distance from each other, and can bind into dimers.

We consider the classical three-body hard-core model in two and three dimensions. To obtain the infinite-pressure

(a) tommaso.comparin@ens.fr
(b) sebastian.kapfer@fau.de
(c) werner.krauth@ens.fr

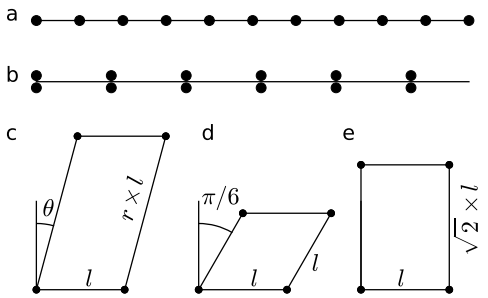

Fig. 1: Close-packed structures in 1D and 2D. (a) Linear array of isolated atoms and (b) of dimers with the smallest spacing allowed by the three-body cut-off. (c) General case of the 2D oblique lattice structure, (d) triangular lattice at $(r, \theta) = (1, \pi/6)$, (e) rectangular lattice with $(r, \theta) = (\sqrt{2}, 0)$.

limit, we first solve heuristically the three-body equivalent of the classic sphere-packing problem [3]: We maximise the packing fraction for several families of structures where the three-body constraint eq. (1) is tight. We support our result by simulated-annealing calculations which confirm our highest-density close-packed structures. In two dimensions, the densest structure is a triangular lattice of dimers, while in three dimensions it is a simple-hexagonal lattice of isolated atoms. Finally, we use Monte Carlo (MC) simulations in the NPT ensemble to determine the phase diagram at finite pressure. Both in 2D and 3D, we find no other stable thermodynamic phases besides the liquid and the high-density solid.

Close-packed structures. – We illustrate our procedure to compute densities of close-packed structures in the one-dimensional case. We consider evenly spaced lattice sites with lattice constant l. For a lattice with a single atom on every site – fig. 1(a) – the smallest triplet is composed by three subsequent sites and the hard-core condition in eq. (1) leads to the following bound on the lattice spacing:

$$R = \sqrt{\frac{l^2 + l^2 + (2l)^2}{3}} = l\sqrt{2} \geq R_0. \qquad (2)$$

The corresponding upper bound on the density ρ reads $\rho \leq \rho_{\max} = \sqrt{2}/R_0$. On the other hand, for the lattice with every site occupied by a dimer of two atoms, the smallest triplet consists of a dimer and an additional atom on a neighbouring site; the root-mean-square distance is $R = l\sqrt{2/3}$ and the close-packed density is $\rho_{\max} = 2\sqrt{2/3}/R_0$. Thus, at high pressure, the dimer lattice is favoured (see table 1).

In two dimensions, we consider the family of oblique lattices – see fig. 1(c) – in which the unit cell is a parallelogram with edges l and $r \times l$, and where the smaller internal angle equals $\pi/2 - \theta$. Without loss of generality, we set $r \geq 1$ and $0 \leq \theta \leq \arcsin(1/(2r))$. This family includes the triangular and the rectangular lattices, as indicated in figs. 1(d) and 1(e). For isolated particles, close packing is obtained for a rectangular lattice with aspect ratio $\sqrt{2}$, while for dimers, the close-packed structure is a triangular lattice. Again, high pressure favours the formation of dimers (see table 1).

Table 1: Densities of D-dimensional close-packed structures. The structure may include free parameters (aspect ratio r or angle θ), and the optimal values are indicated. Labels a and d correspond to filling the lattice sites with atoms or dimers, respectively.

D	structure	param.	$\rho_{\max} R_0^D$	
1	regular spacing a	–	$\sqrt{2}$	1.41
	regular spacing d	–	$2\sqrt{2/3}$	**1.63**
2	oblique a	$r = \sqrt{2}$ $\theta = 0$	$\sqrt{2}$	1.41
	oblique d	$r = 1$ $\theta = \pi/6$	$(2/\sqrt{3})^3$	**1.54**
3	Barlow ABA a	$r = 1/2$	$\frac{13}{27}\sqrt{26/3}$	1.42
	Barlow ABA d	$r = \sqrt{2/3}$	$(2/\sqrt{3})^3$	1.54
	Barlow ABC a	$r = 1/\sqrt{6}$	$(2/\sqrt{3})^3$	1.54
	Barlow ABC d	$r = \sqrt{2/3}$	$(2/\sqrt{3})^3$	1.54
	tetragonal a	$r = 1$	$(2/\sqrt{3})^3$	1.54
	tetragonal d	$r = 1$	$\sqrt{32/27}$	1.09
	simple-hex. a	$r = 1/\sqrt{2}$	$2\sqrt{2/3}$	**1.63**
	simple-hex. d	$r = 1$	$8\sqrt{2}/9$	1.26

In three dimensions, we consider three families of structures: Barlow, tetragonal, and simple-hexagonal. Barlow packings are the solutions of the conventional (two-body) sphere packing problem and include the fcc and hcp structures [3]. In our case, the lattice parameters are regulated by the three-body hard-core repulsion and not by the hard-sphere diameter. Within this class, we consider A-B-A and A-B-C stackings of triangular lattice planes, with a ratio r between the interplanar spacing and the in-plane lattice constant. For the tetragonal structures, we stretch the simple cubic lattice along the z direction by an aspect ratio r. Finally, we consider the simple-hexagonal structure, which is an A-A-A stacking of triangular lattice planes. As for the Barlow structures, the ratio r between the interplanar and in-plane spacings is a free parameter. Among the 3D structures considered, the highest density is achieved by single particles in a simple-hexagonal lattice with an aspect ratio $r = 1/\sqrt{2}$.

The formation of a structure with more than one particle per lattice site is a peculiarity of systems in which interparticle distances can vanish [23]. In the three-body hard-core model, close-packed systems with dimers are only favourable in low dimensions, as we now show by a heuristic argument: For lattices in which the three closest sites are all equidistant from each other (examples are the two-dimensional triangular lattice and the three-dimensional hcp or fcc lattices), we compute the scaling of the packing density with dimensionality D. We find

$\rho_{\max}(\text{dimers})/\rho_{\max}(\text{atoms}) = 2(2/3)^{D/2}$. Thus, a lattice of dimers is favourable only for $D \leq 3$, while in higher dimensions the density of the atomic lattice is larger. (This argument ignores next-nearest neighbours and non-uniform distances between lattice sites.) The same scaling argument can be generalised to a hard-core k-body model on a lattice in which the closest k sites are all at the same distance with each other. Up to $(k-1)$ particles can share a lattice site. As in the $k = 3$ case, for large D the largest density is obtained for isolated atoms.

From the list of densities in table 1, we infer that the close-packed structures – in the classes considered here – of the three-body hard-core model are a regular lattice of dimers in $D = 1$, a triangular lattice of dimers in $D = 2$, and a simple-hexagonal lattice of single particles in $D = 3$. Our approach is not exhaustive, and does not constitute a proof. In particular, mixtures of atoms and dimers remain to be explored. We support our results using a simulated-annealing procedure [24, 25], in which we perform subsequent short MC simulations at slowly increasing pressure, starting from low-density disordered configurations. Simulated annealing runs for $N = 100, 72, 64$ particles in $D = 1, 2, 3$ dimensions, respectively, indeed yield the expected structures in the limit of infinite pressure.

Finite-pressure results. – We now consider the phase diagram of the three-body hard-core model at finite pressure. We use a Markov-chain MC scheme to simulate the system in the NPT ensemble (at fixed particle number N and pressure P). Our MC scheme involves two kinds of moves. The first is the standard local move, where a randomly chosen particle is displaced in its neighbourhood, and the move is accepted unless it violates any of the three-body constraints of eq. (1). The second move is a change of volume that also modifies the shape of the simulation box: For a D-dimensional box with edges $L_1, .., L_D$, the move modifies one of the L's by adding or removing a random amount of void space (a rectangle aligned with the coordinate axes, constrained to touch a randomly chosen particle). This move does not alter the positions of the particles. As an example, if particle k and direction 1 are chosen, one move corresponds to removing the D-dimensional portion of space defined by $\{(x_1, .., x_D) \mid x_{k,1} < x_1 < x_{k,1} + \delta_1\}$, where δ_1 is chosen randomly in a fixed interval. This move, which changes L_1 into $L_1 - \delta_1$, is accepted only if it does not remove any particle and if the new configuration still satisfies the three-body constraint. The complementary move consists in extending L_1 to $L_1 + \delta_1$, by adding a portion of empty space with edges $\delta_1 \times L_2 \times .. \times L_D$, starting from $x_{k,1}$. The acceptance probability for this insertion move is $p_{\text{acc}} = \exp(-\beta P \Delta V)$, where $\Delta V = \delta_1 \Pi_{i=2}^{D} L_i$ is the change in volume; this differs from the conventional NPT move, which rescales the simulation box and the particle positions and requires an additional factor V^N in the statistical weight. In addition to the mentioned acceptance conditions, we reject moves that lead to very elongated box shapes, $\max_{i,j}(L_i/L_j) > 2$, as is common in MC methods based on variable box shape [26–28] to avoid strong finite-size effects.

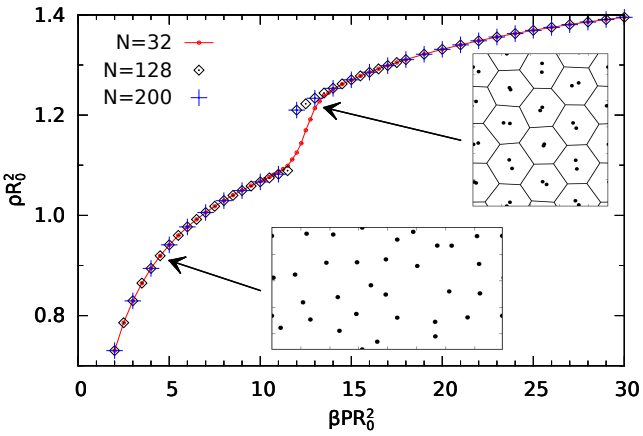

Fig. 2: (Colour on-line) Equation of state (density vs. pressure) for the 2D three-body hard-core system, with different system size N. The insets show snapshots of the $N = 32$ system at pressures $\beta P R_0^2 = 4.5$ and $\beta P R_0^2 = 13$. Black lines in the inset indicate Voronoi cells of the dimer centres of mass.

Two-dimensional system. For the $D = 2$ system, we expect a disordered isotropic liquid phase at low pressure and a triangular solid phase of dimers at high pressure. We initialise the MC sampling with configurations in the solid phase, and observe melting for low values of P. Melting is indeed observed as a jump in the density, as shown in the equation of state (fig. 2). For small systems ($N = 32$), there is an intermediate pressure regime where the system oscillates between the two phases. For larger systems, we only observe a single phase at each pressure, and the specific volume no longer has a bimodal distribution – see fig. 3(a). The density gap indicates a first-order phase transition, for the system sizes under study.

In the solid phase, defects are suppressed in our simulations due to the system sizes considered. The density in the equation of state, fig. 2, overestimates infinite-system value (with defects). In particular, vacancies are not observed on our simulation time scales, even though our volume- and shape-changing move can in principle create the void space for a new lattice row to form (which has been advanced as a mechanism to change the number of lattice sites [29]).

Moreover, in two dimensions, the Mermin-Wagner theorem [30] precludes the existence of a crystal with truly long-ranged positional order, but allows for a solid phase with long-ranged orientational order and algebraically decaying positional order. 2D systems frequently exhibit an intermediate hexatic phase with short-ranged positional order, such as recently shown for hard disks [31, 32] and soft disks [33]. Since the dimers in our system effectively interact as hard disks (see below), an intermediate hexatic phase of dimers might also exist here, and could be

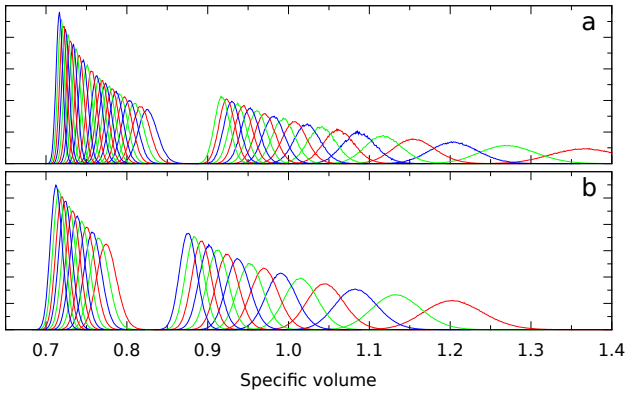

Fig. 3: (Colour on-line) Probability density function of the specific volume $V/(NR_0^D)$ at fixed pressure. (a) $N = 128$ particles in $D = 2$ dimensions, (b) $N = 64$ particles in $D = 3$ dimensions. Pressures are as in figs. 2 and 8, respectively.

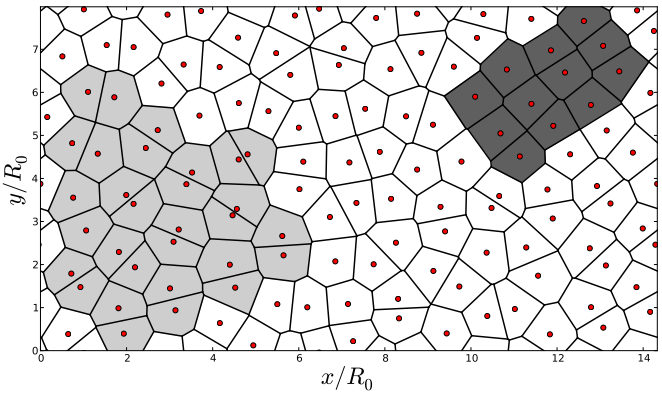

Fig. 4: (Colour on-line) Snapshot of $N = 128$ particles (red dots) at $\beta P R_0^2 = 14$, during the equilibration of a simulation started from a low-density disordered configuration. Black lines represent the particles' Voronoi cells. A patch with rectangular order is highlighted in dark gray, while a nucleating dimer solid is highlighted in light gray.

observable in larger simulations.

From table 1 we identify a further candidate for an intermediate phase between the monomer liquid and the dimer solid: The rectangular close-packed structure of monomers attains a density only 10% below the close-packed triangular lattice of dimers. In our simulations, we observe transient patches with rectangular order: fig. 4 shows both the nucleating dimer solid and a rectangular patch. The aspect ratio of the rectangles is consistent with the close-packed structure, *i. e.*, $r = \sqrt{2}$. However, we find no pressure at which the rectangular structure is the equilibrium phase. Instead, the rectangular patches seem to decay by coalescence of two neighbouring lattice rows into a line of dimers, eventually forming a triangular dimer patch. Conversely, a dimer liquid was found to be unstable and to decompose.

Quantitatively, we define the term *dimer* to describe two particles that are each other's closest neighbour. This definition applies also to the disordered phase, where not all particles participate in tightly bound pairs. We measure the dimer fraction $2N_\mathrm{d}/N$ according to this definition (where N_d is the number of dimers), and we show in fig. 5(a) that in the liquid, this quantity strongly deviates from its ideal-solid value of 1. Melting of the solid phase and decomposition of the dimers thus occurs in a single step.

The three-body model with all particles paired up into small dimers can be mapped to a conventional two-body hard-core system, containing composite particles (the dimers). In the infinite-pressure limit, dimers have zero extent and the dimer-dimer interaction makes them equivalent to hard disks with an effective radius $\sigma = R_0\sqrt{3/8}$. At finite pressure, this mapping is approximate. In fig. 6(a), we compare the equation of state for 128 three-body-interacting particles and 64 hard disks. After rescaling the pressure by a factor of two stemming from the $2N$-dimensional configuration space of the three-body particles vs. the $2N_\mathrm{disks} = N$ dimensions for the hard disks, the equations of state agree fairly well in the solid phase. The density of hard disks is systematically larger, as due to the non-zero extent of the dimers at finite pressure. This deviation decreases for increasing pressure.

In analogy with the hard-disk model, we define the orientational order parameter of the liquid–solid transition. We identify the N_j neighbours of the j-th dimer (where $N_j = 6$ in the ideal crystal) through a Voronoi tessellation. The *local* orientational order parameter is then [34]

$$\psi_{6,j} = \frac{\sum_{k=1}^{N_j} W_{jk} \exp(6\mathrm{i}\theta_{jk})}{\sum_{k=1}^{N_j} W_{jk}}, \tag{3}$$

where θ_{jk} is the angle of the vector $\mathbf{r}_j - \mathbf{r}_k$ with respect to a reference axis and W_{jk} is the length of the Voronoi boundary between dimers j and k. The *global* orientational order parameter is $\Psi_6 = |\sum_{j=1}^{N_\mathrm{d}} \psi_{6,j}|/N_\mathrm{d}$. In the solid phase this quantity remains finite for increasing system sizes – fig. 5(c) – while in the fluid phase it decays as $1/\sqrt{N_\mathrm{d}}$ and hexagonal order for the residual dimers is lost. In fig. 6(b), we show the global orientational order parameter Ψ_6 for the three-body hard-core system and its hard-disk analogue. Within our accuracy, the decomposition of dimers and the melting of the hard disks take place at the same pressure.

At finite pressure, the size of the dimers remains finite. It is thus interesting to study dimer orientation as an effective spin model. Dimers can rotate in 2D and have twofold rotational symmetry. We define the dimer magnetisation m as

$$m = \frac{1}{N_\mathrm{d}} \left| \sum_{j=1}^{N_\mathrm{d}} \exp(2\mathrm{i}\alpha_j) \right| \tag{4}$$

where α_j is the angle that the dimer forms with a reference axis.

We first consider four particles paired up into two dimers of fixed size, and free to rotate about their centres of mass,

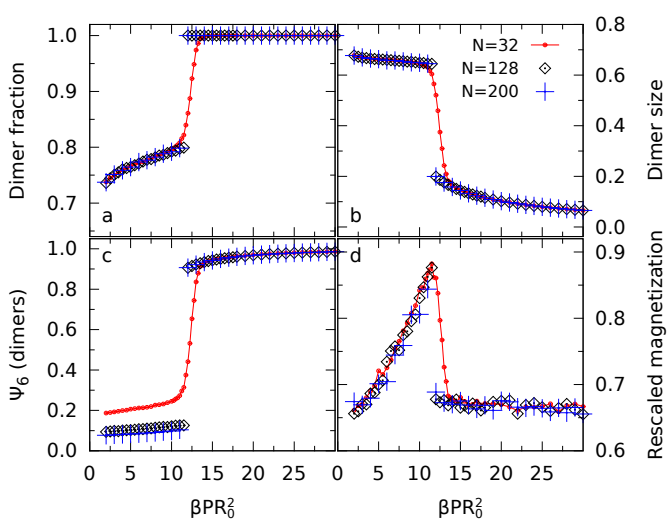

Fig. 5: (Colour on-line) Symbols and colours as in fig. 2. (a) Fraction $2N_{\rm d}/N$ of dimers in the system. (b) Average dimer size, in units of R_0. (c) Ψ_6 order parameter of dimers. (d) Dimer magnetisation m, multiplied by $\sqrt{N_{\rm d}}$ (statistical uncertainties are comparable to symbol sizes).

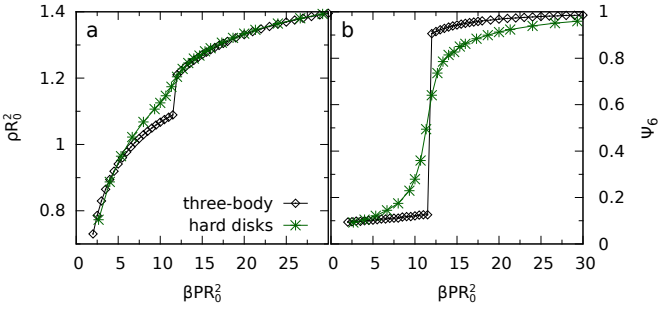

Fig. 6: (Colour on-line) The three-body hard-core solid compared to hard disks: (a) Equation of state and (b) global orientational order parameter Ψ_6 for $N = 128$ three-body-interacting particles (black diamonds) and $N_{\rm disks} = 64$ hard-disks (green stars). The conversion from hard-disk to three-body units follows from $\sigma = R_0\sqrt{3/8}$; the density and packing fraction of the effective model read $\rho_{\rm disks} = \rho/2$ and $\eta_{\rm disks} = \rho_{\rm disks}\pi\sigma^2 = \rho R_0^2 3\pi/16$, while the pressure is $P_{\rm disks}\sigma^2 = 2(8/3)PR_0^2$. Data for the three-body model (ρ and Ψ_6) are the same as in figs. 2 and 5(c).

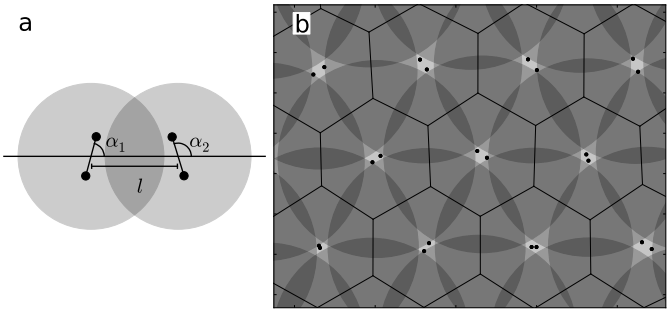

Fig. 7: (a) Representation of the configuration of four particles (dots) paired up in two dimers. Each shaded circle represents the excluded region generated by the two particles in a dimer. (b) Partial snapshot of the simulation of $N = 128$ particles at $\beta PR_0^2 = 20$. For each dimer, the excluded region is shaded. Black lines indicate Voronoi cells of the dimer centres of mass.

as shown in fig. 7(a). Each dimer generates a circular region around its centre of mass into which none of the two particles of the other dimer can penetrate. The radius of the excluded region depends on the dimer's size. When approaching each other, the dimers can no longer rotate freely and have to progressively align with each other, standing perpendicular to the dimer–dimer axis ($\alpha_1, \alpha_2 = \pi/2$). In the triangular lattice, this interaction is frustrated, since not all pairs of dimers in a triangle can align. The dimers then have to shrink to satisfy the three-body constraint (see fig. 7(b)). Effectively, the dimer spins are noninteracting, and their magnetisation vanishes as $1/\sqrt{N_{\rm d}}$ as the system size increases. This is confirmed by the collapse of the $m\sqrt{N_{\rm d}}$ curves – see fig. 5(d). In the thermodynamic limit, no magnetic order remains. In fig. 5(b) we show that the average size of dimers in the solid phase keeps decreasing, as required.

Three-dimensional system. Our simulations in three dimensions are analogous to the $D = 2$ simulations described above. Starting from the ideal simple-hexagonal solid, at low pressure the system melts into a disordered liquid phase; the equation of state is shown in fig. 8. As in the two-dimensional case, the gap in the specific-volume probability distribution shows that for this system size, the transition is discontinuous – see fig. 3(b).

We quantify local structure using bond order parameters [35], again following the construction of ref. [34] (*i. e.*, we weight the contribution of each bond between neighbours with the area of the shared Voronoi facet). In the solid phase, the distributions of q_4 and q_6 (see inset of fig. 8) are peaked, and their averages approach the perfect-lattice limit at high pressure. In the liquid phase, these distributions are broader, and give no indication for preferred local configurations. Except at the melting pressure, the distributions evolve smoothly with P, and there is no sign of further structural transformations.

Conclusions. – In this paper, we have studied the classical three-body hard-core model in two and three dimensions, and identified a unique solid phase in both cases.

In two dimensions, the transition involves simultaneous appearance of two types of order: particles form dimers, and the dimers order in a triangular solid that we expect to have quasi-longrange positional order.

The solid phase can be mapped to an effective hard-disk model, which reproduces the equation of state for large enough pressure. Dimers break up right at the melting transition of the effective hard-disks. The small system sizes considered here do not allow us to comment on the existence of an intermediate hexatic phase of dimers. Moreover, we note that the dimer solid phase does not

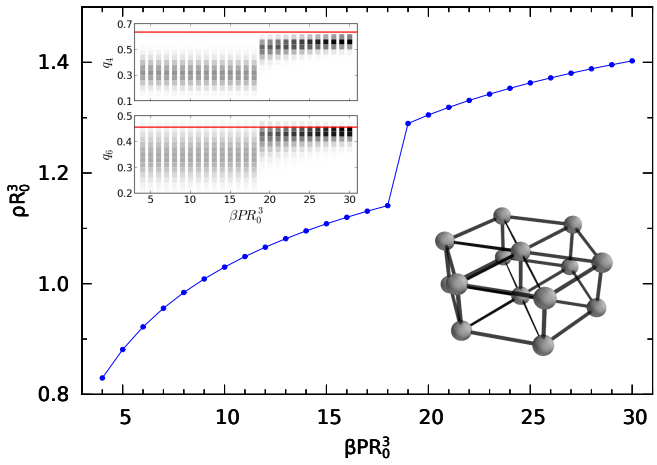

Fig. 8: (Colour on-line) Main panel: Equation of state (density vs. pressure) for the 3D three-body hard-core model of $N = 64$ particles. Inset (left): q_4 and q_6 histograms, for each pressure value (darker bins correspond to higher probability), and perfect-lattice limit (red line). Inset (right): representation of the simple-hexagonal lattice (realised at high pressure).

show (magnetic) order of dimer orientations. We explain this feature through the frustration of the effective spin-spin interaction that results from the three-body cut-off.

In three dimensions, the close-packed structure is formed by isolated particles – rather than tightly bound dimers – placed on a simple-hexagonal lattice. This has an interest in connection with the model for the unitary Bose gas, since pairs of particles at very small distances would be pathological in the original quantum model [17]. Our equation of state enriches the phase diagram in ref. [17] at high temperature and pressure, and one might be able to link these two different regimes for the model.

More generally, the nature of the highest-density structure in the three-body hard-core model might represent a mathematically non-trivial generalisation of the classic Kepler problem [3], both in two and in three dimensions.

Acknowledgments. – We thank Riccardo Rossi for helpful discussions.

REFERENCES

[1] D. Szász (Editor), *Hard Ball Systems and the Lorentz Gas* (Springer-Verlag, Berlin Heidelberg) 2000.
[2] J. H. Conway and N. J. A. Sloane, *Sphere Packings, Lattices and Groups* (Springer-Verlag, New York) 1999.
[3] T. Aste and D. Weaire, *The pursuit of perfect packing* (Institute of Physics Publishing, Bristol) 2000.
[4] W. Glöckle, H. Witała, D. Hüber, H. Kamada and J. Golak, *Phys. Rep.*, **274** 107 (1996).
[5] E. Epelbaum, H.-W. Hammer and Ulf-G. Meissner, *Rev. Mod. Phys.*, **81** 1773 (2009).
[6] D. J. Gross and M. Mezard, *Nucl. Phys. B*, **240** 431 (1984).
[7] D. S. Petrov, *Phys. Rev. Lett.*, **112** 103201 (2014).
[8] V. Efimov, *Phys. Lett. B*, **33** 563 (1970).
[9] T. Kraemer, M. Mark, P. Waldburger, J. G. Danzl, C. Chin, B. Engeser, A. D. Lange, K. Pilch, A. Jaakkola, H.-C. Nägerl and R. Grimm, *Nature*, **440** 315 (2006).
[10] M. Zaccanti, B. Deissler, C. D'Errico, M. Fattori, M. Jona-Lasinio, S. Müller, G. Roati, M. Inguscio and G. Modugno, *Nature Phys.*, **5** 586 (2009).
[11] S. E. Pollack, D. Dries and R. G. Hulet, *Science*, **326** 1683 (2009).
[12] B. S. Rem, A. T. Grier, I. Ferrier-Barbut, U. Eismann, T. Langen, N. Navon, L. Khaykovich, F. Werner, D. S. Petrov, F. Chevy and C. Salomon, *Phys. Rev. Lett.*, **110** 163202 (2013).
[13] R. J. Fletcher, A. L. Gaunt, N. Navon, R. P. Smith and Z. Hadzibabic, *Phys. Rev. Lett.*, **111** 125303 (2013).
[14] P. Makotyn, C. E. Klauss, D. L. Goldberger, E. A. Cornell and D. S. Jin, *Nature Phys.*, **10** 116 (2014).
[15] J. von Stecher, *J. Phys. B: At. Mol. Opt. Phys.*, **43** 101002 (2010).
[16] Y. Yan and D. Blume, *Phys. Rev. A*, **90** 013620 (2014).
[17] S. Piatecki and W. Krauth, *Nat. Commun.*, **5** 3503 (2014).
[18] M. Rossi, L. Salasnich, F. Ancilotto and F. Toigo, *Phys. Rev. A*, **89** 041602(R) (2014).
[19] L. H. Thomas, *Phys. Rev.*, **47** 903 (1935).
[20] M. Berninger, A. Zenesini, B. Huang, W. Harm, H. C. Nägerl, F. Ferlaino, R. Grimm, P. S. Julienne and J. M. Hutson, *Phys. Rev. Lett.*, **107** 120401 (2011).
[21] R. J. Wild, P. Makotyn, J. M. Pino, E. A. Cornell and D. S. Jin, *Phys. Rev. Lett.*, **108** 145305 (2012).
[22] J. Wang, J. P. D'Incao, B. D. Esry and C. H. Greene, *Phys. Rev. Lett.*, **108** 263001 (2012).
[23] B. M. Mladek, D. Gottwald, G. Kahl, M. Neumann and C. N. Likos, *Phys. Rev. Lett.*, **96** 045701 (2006).
[24] S. Kirkpatrick, Jr. C. D. Gelatt and M. P. Vecchi, *Science*, **220** 671 (1983).
[25] V. Černy, *J. Optim. Theory Appl.*, **45** 41 (1985).
[26] L. Filion, M. Marechal, B. van Oorschot, D. Pelt, F. Smallenburg and M. Dijkstra, *Phys. Rev. Lett.*, **103** 188302 (2009).
[27] J. de Graaf, L. Filion, M. Marechal, R. van Roij and M. Dijkstra, *J. Chem. Phys.*, **137** 214101 (2012).
[28] E. Bianchi, G. Doppelbauer, L. Filion, M. Dijkstra and G. Kahl, *J. Chem. Phys.*, **136** 214102 (2012).
[29] W. C. Swope and H. C. Andersen, *Phys. Rev. A*, **46** 4539 (1992).
[30] N. D. Mermin and H. Wagner, *Phys. Rev. Lett.*, **17** 1307 (1966).
[31] E. P. Bernard and W. Krauth, *Phys. Rev. Lett.*, **107** 155704 (2011).
[32] M. Engel, J. A. Anderson, S. C. Glotzer, M. Isobe, E. P. Bernard and W. Krauth, *Phys. Rev. E*, **87** 042134 (2013).
[33] S. C. Kapfer and W. Krauth, *Phys. Rev. Lett.*, **114** 035702 (2015).
[34] W. Mickel, S. C. Kapfer, G. E. Schröder-Turk and K. Mecke, *J. Chem. Phys.*, **138** 044501 (2013).
[35] P. Steinhardt, D. R. Nelson and M. Ronchetti, *Phys. Rev. B*, **28** 784 (1983).